Supplementary Information: Future Changes in Severe Frontal Precipitation Events over Europe and Their Drivers

Armin Schaffer[1], Albert Ossó[1], and Douglas Maraun[1]

[1]Wegener Center for Climate and Global Change, University of Graz, Graz, Austria

Correspondence: Armin Schaffer (armin.schaffer@uni-graz.at)

Table 1. Overview of all datasets used in this study, including horizontal resolution, number of available pressure levels and associated sub-ensemble classification and global mean surface temperature change (ΔGMST).

RCM	GCM	Sub-ensemble	Resolution [°]	Number of levels	ΔGMST (DJF, JJA) [K]
ALADIN63	CNRM-CERFACS-CNRM-CM5	CORDEX	0.11 × 0.11	5[a]	3.5, 3.1
ALADIN63	MOHC-HadGEM2-ES	CORDEX	0.11 × 0.11	5[a]	4.6, 4.1
ALADIN63	MPI-M-MPI-ESM-LR	CORDEX	0.11 × 0.11	5[a]	3.5, 3.2
ALADIN63	NCC-NorESM1-M	CORDEX	0.11 × 0.11	5[a]	3.1, 2.9
COSMO-crCLIM-v1-1	CNRM-CERFACS-CNRM-CM5	CORDEX	0.11 × 0.11	8[b]	3.5, 3.1
COSMO-crCLIM-v1-1	MOHC-HadGEM2-ES	CORDEX	0.11 × 0.11	8[b]	4.6, 4.1
COSMO-crCLIM-v1-1	MPI-M-MPI-ESM-LR	CORDEX	0.11 × 0.11	8[b]	3.5, 3.2
COSMO-crCLIM-v1-1	NCC-NorESM1-M	CORDEX	0.11 × 0.11	8[b]	3.1, 2.9
COSMO-crCLIM-v1-1	ICHEC-EC-EARTH	CORDEX	0.11 × 0.11	8[b]	3.5, 3.1
	NorESM2-LM	CMIP6-LR	1.875 × 2.5	33 / 23[c]	3.2, 3.2
	MPI-ESM1-2-LR	CMIP6-LR	1.875 × 1.875	33 / 23[c]	3.2, 2.9
	IPSL-CM6A-LR	CMIP6-LR	1.25 × 2.5	33 / 23[c]	4.8, 4.7
	MIROC6	CMIP6-LR	1.4 × 1.4	33 / 23[c]	3.2, 2.8
	MRI-ESM2-0	CMIP6-HR	1.125 × 1.125	33 / 23[c]	3.7, 3.6
	NorESM2-MM	CMIP6-HR	0.9357 × 1.25	33 / 23[c]	3.3, 3.1
	CMCC-CM2-SR5	CMIP6-HR	0.9357 × 1.25	33 / 23[c]	4.3, 4.2
	CMCC-ESM2	CMIP6-HR	0.9357 × 1.25	33 / 23[c]	4.2, 4.1
	MPI-ESM1-2-HR	CMIP6-HR	0.9375 × 0.9375	33 / 23[c]	3.1, 2.9
	EC-Earth3	CMIP6-HR	0.7031 × 0.7031	33 / 23[c]	4.6, 4.3

[a]925, 850, 700, 500, 200 hPa

[b]925, 850, 700, 600, 500, 400, 300, 200 hPa

[c]1000 – 200 (25 hPa steps), with 10 levels missing geopotential data (725, 675, 625, 575, 525, 475, 425, 375, 325, 275 hPa).

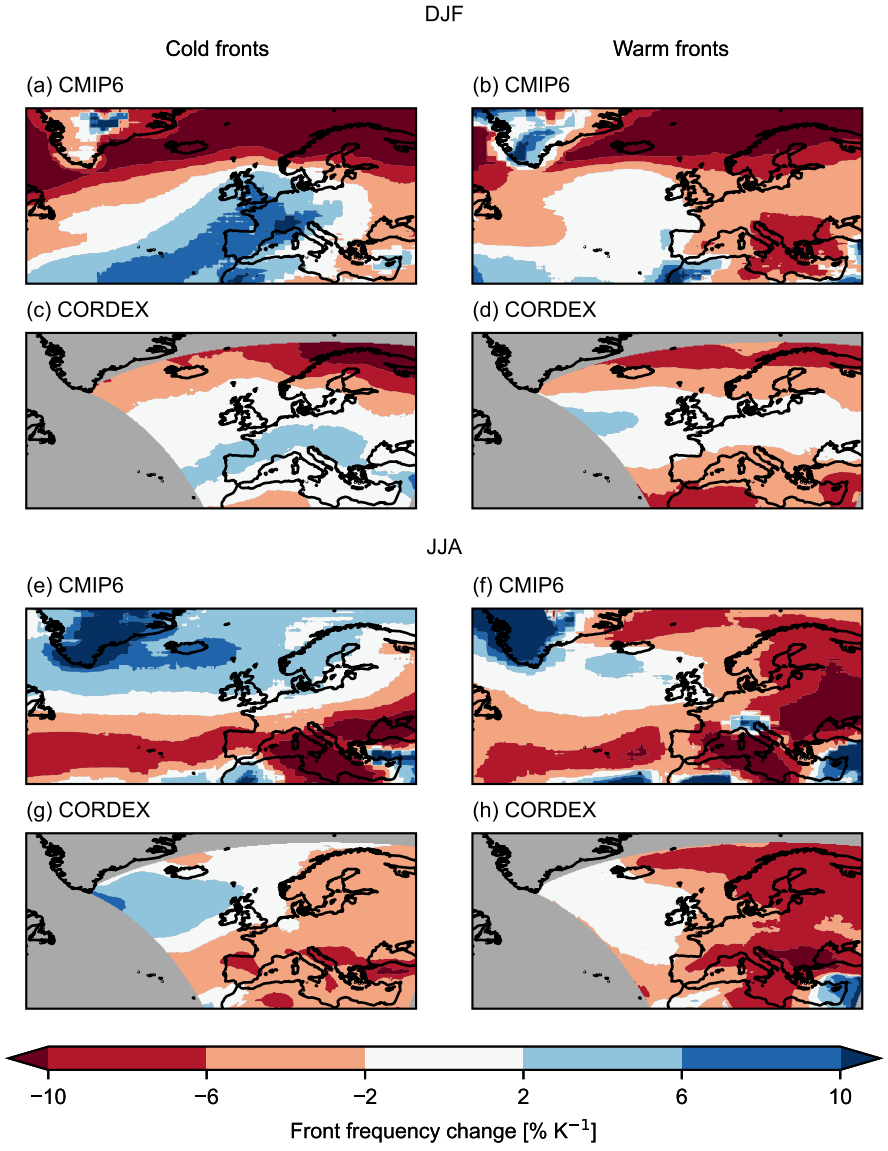

Figure S1. Relative changes in the number of fronts per degree of warming, for DJF (a – b) and JJA (e – h), for cold (a, c, e, g) and warm fronts (b, d, f, h). Panels a, b, e, f display CMIP6 and panels c, d, g, h the CORDEX averages. Areas are shaded gray if they lie outside the EURO-CORDEX domain.

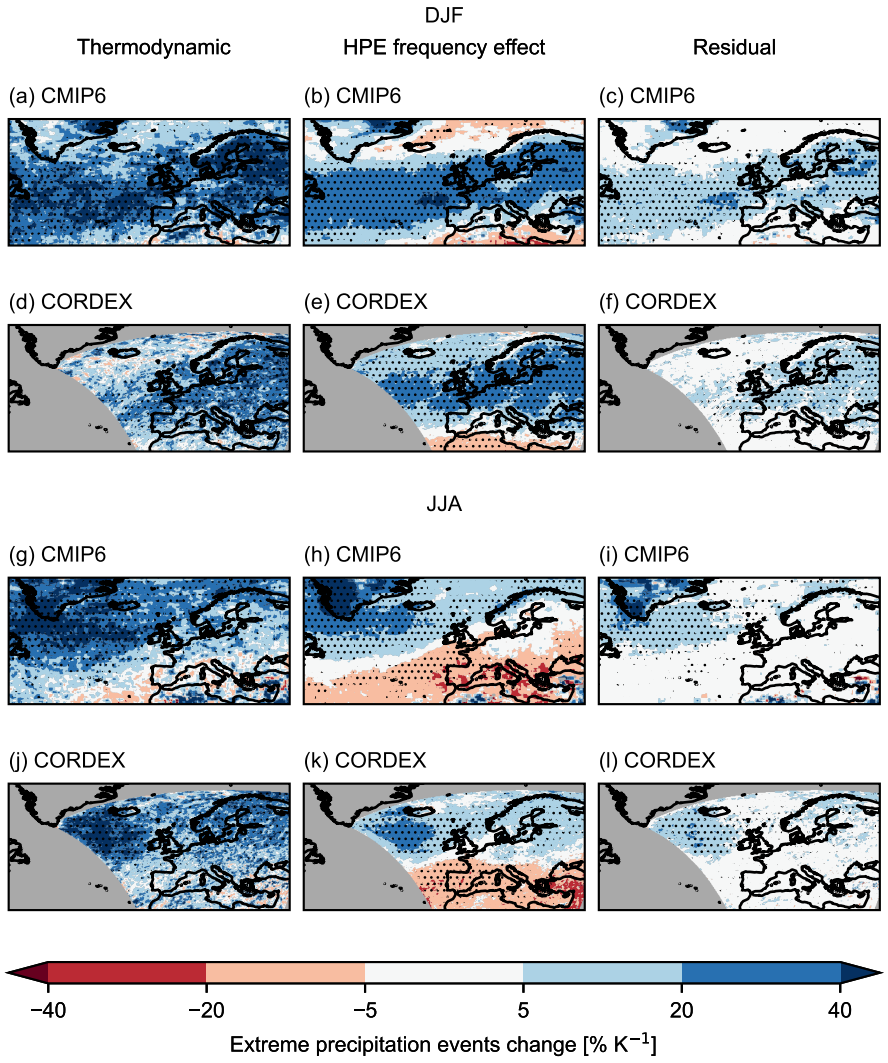

Figure S2. Same as Fig. 3, but the decomposition is carried out by expressing the number of frontal EPE as $N_{\mathrm{EPE}} = N_{\mathrm{HPE}}\, p$, where N_{HPE} is the number of frontal HPEs and p the conditional probability that a HPE is also an EPE.

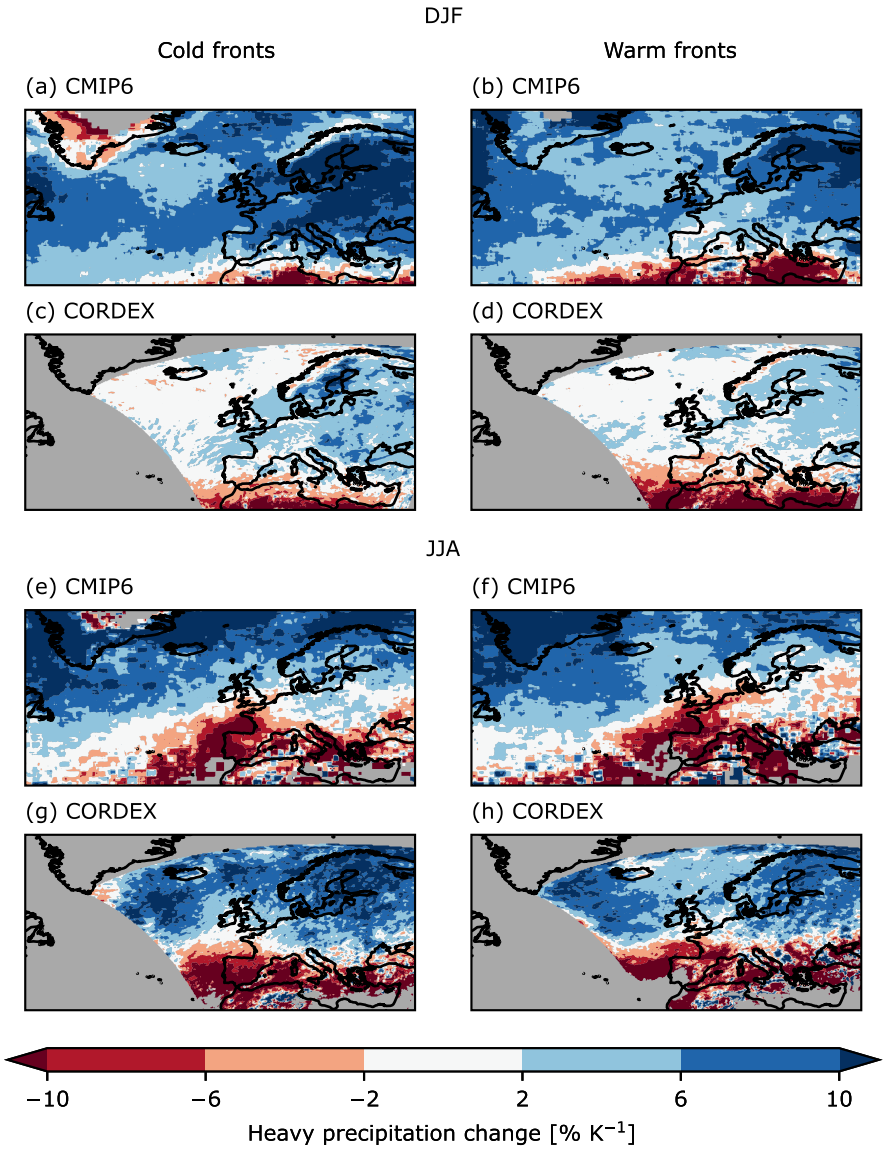

Figure S3. Relative changes of the 99.5th percentile of all 6-hourly precipitation per degree of warming, for DJF (a – b) and JJA (e – h), for cold (a, c, e, g) and warm fronts (b, d, f, h). Panels a, b, e, f display CMIP6 and panels c, d, g, h the CORDEX averages. Areas are shaded gray if the value is below 2 mm in the historical period or they lie outside the EURO-CORDEX domain.

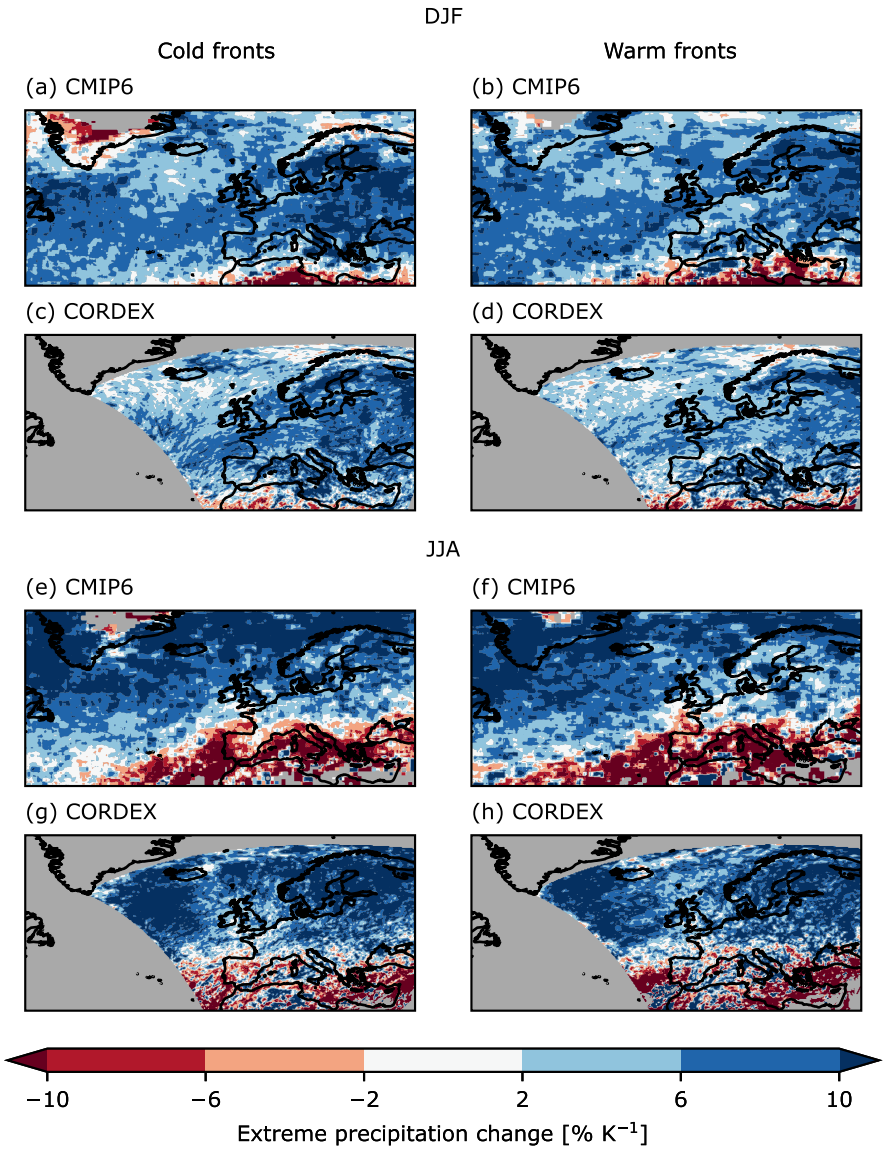

Figure S4. Same as Fig. S3 displaying the change of the 99.95th percentile. Areas are shaded gray if the value is below 5 mm in the historical period or they lie outside the EURO-CORDEX domain.

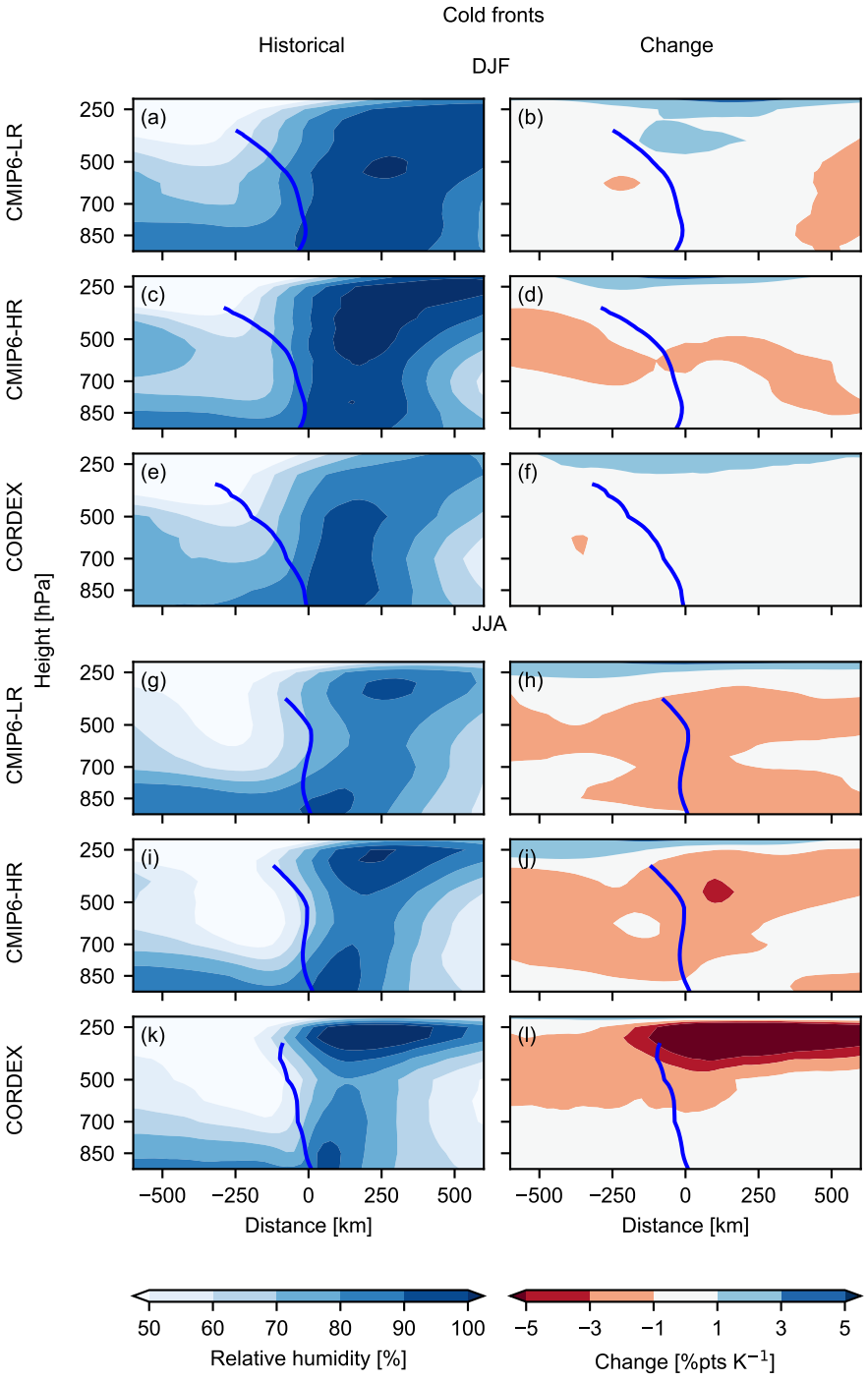

Figure S5. Same as Fig. 4, but showing relative humidity cross-sections of cold fronts for DJF (a – f) and JJA (g – l). Panels (a, c, e, g, i, k) show the values of the historical period in % and (b, d, f, h, j, l) the change per degree of global mean surface warming (%pts K^{-1}).

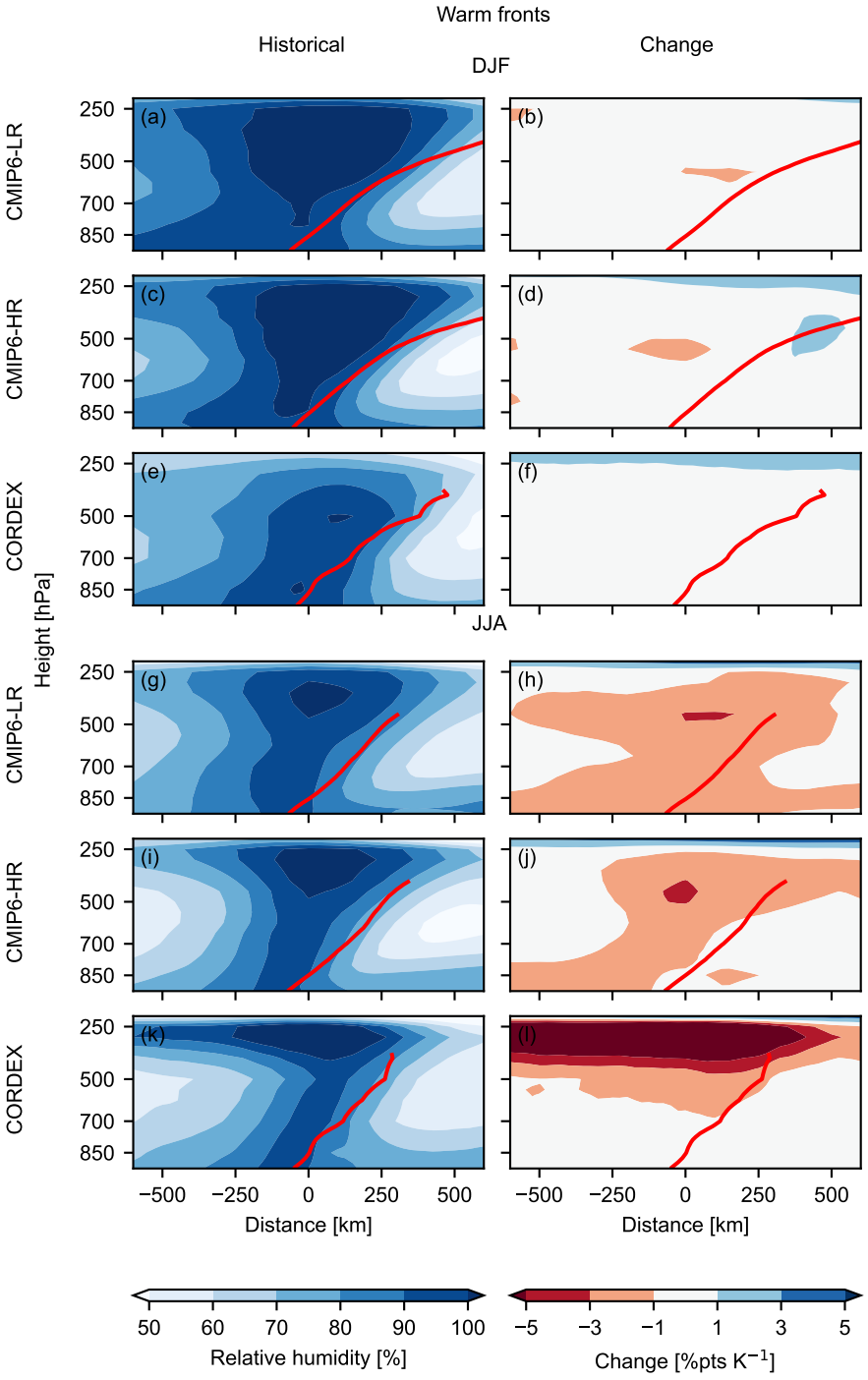

Figure S6. Same as Fig. S5, but showing relative humidity cross-sections of warm fronts.

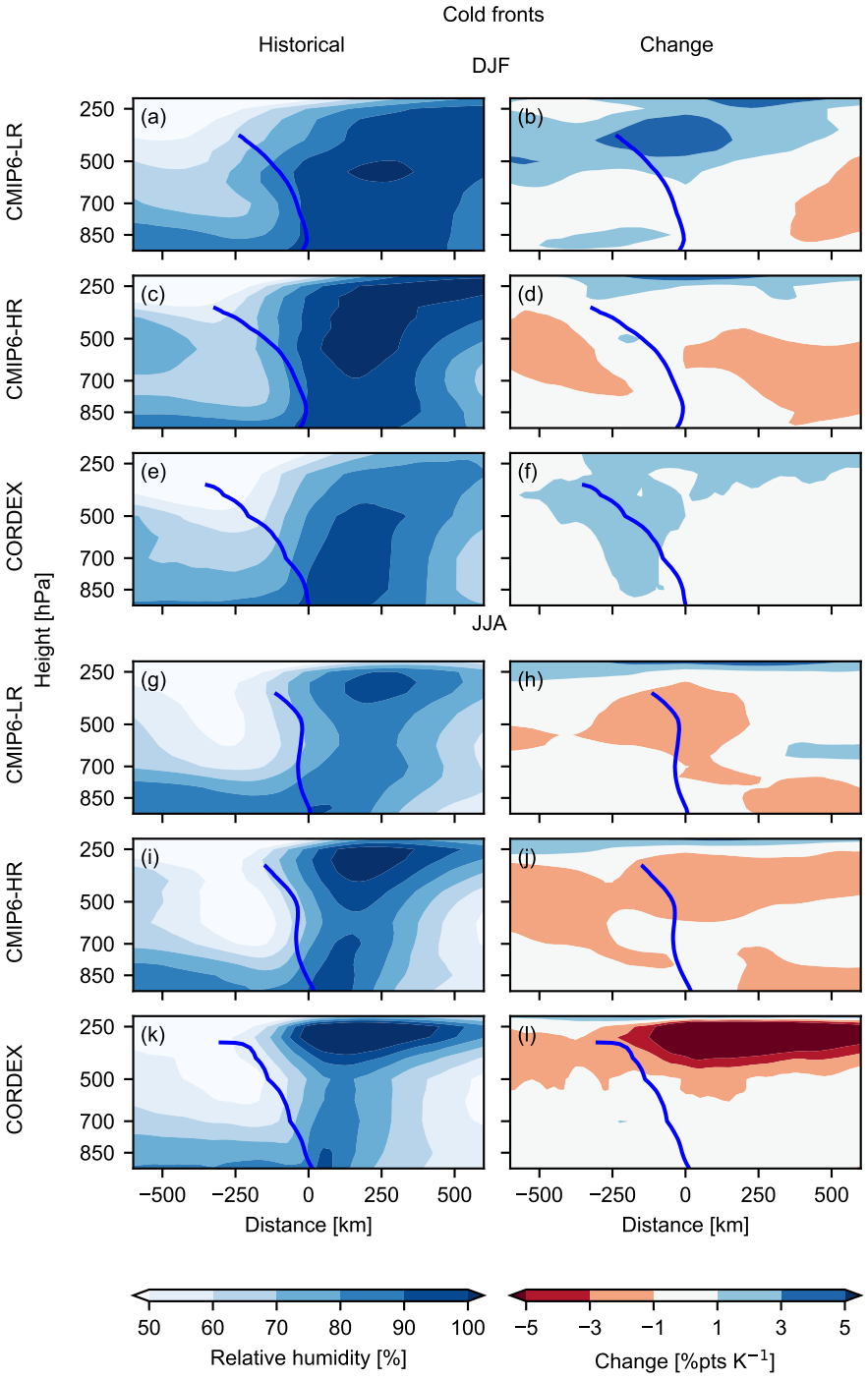

Figure S7. Same as Fig. S5, but showing relative humidity cross-sections of cold fronts of the CEUR region.

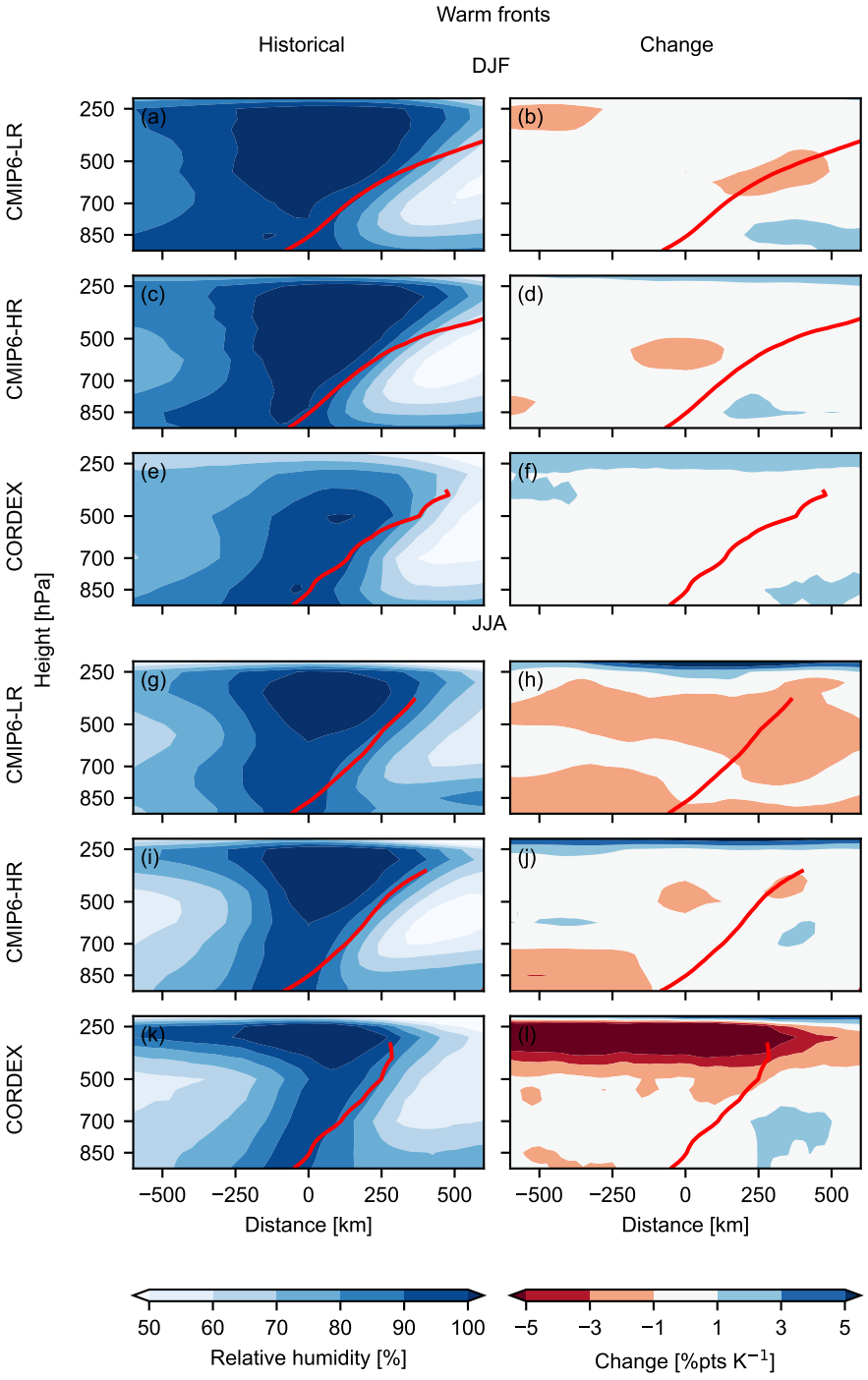

Figure S8. Same as Fig. S5, but showing relative humidity cross-sections of warm fronts of the CEUR region.

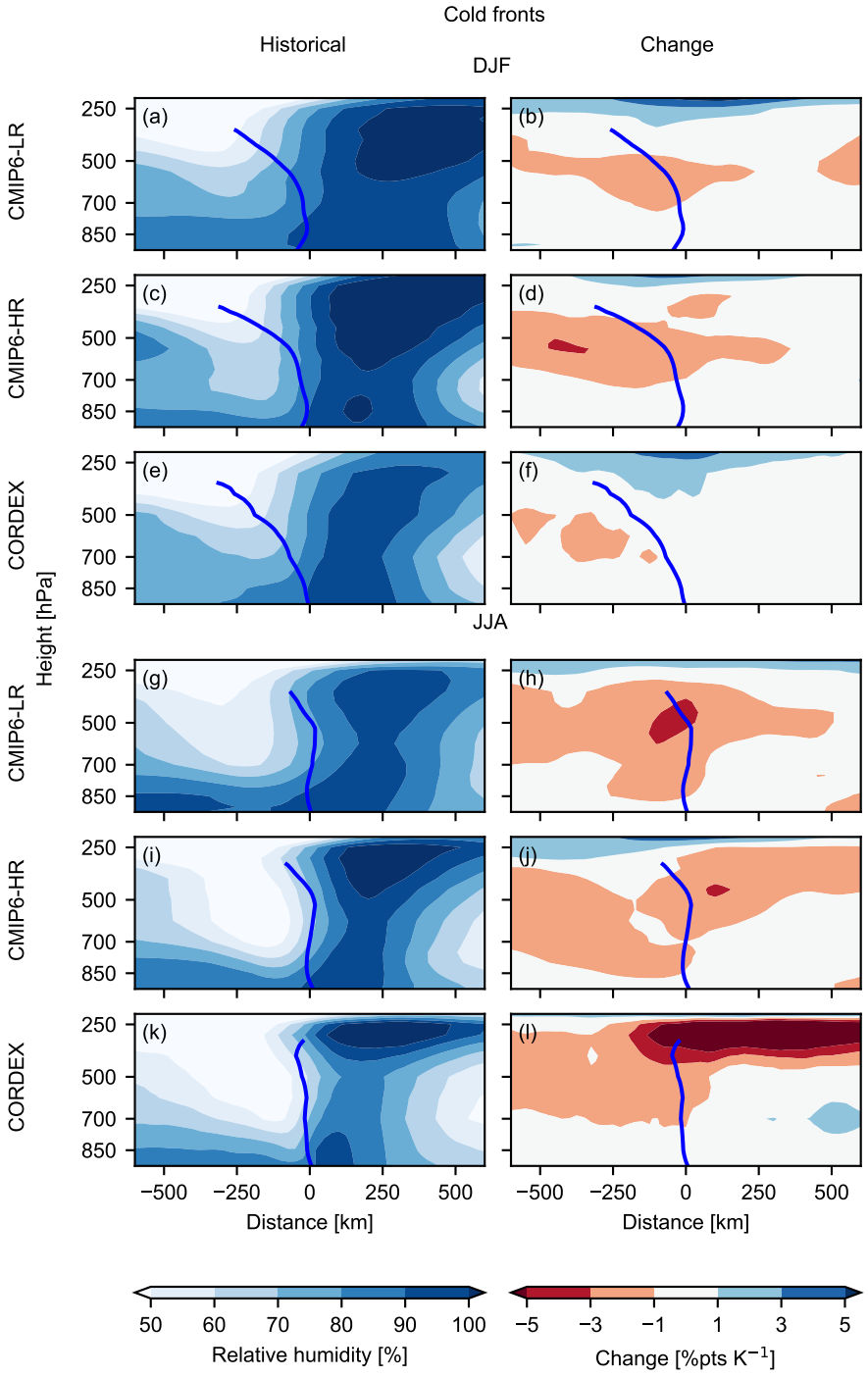

Figure S9. Same as Fig. S5, but showing relative humidity cross-sections of cold fronts of the NWEUR region.

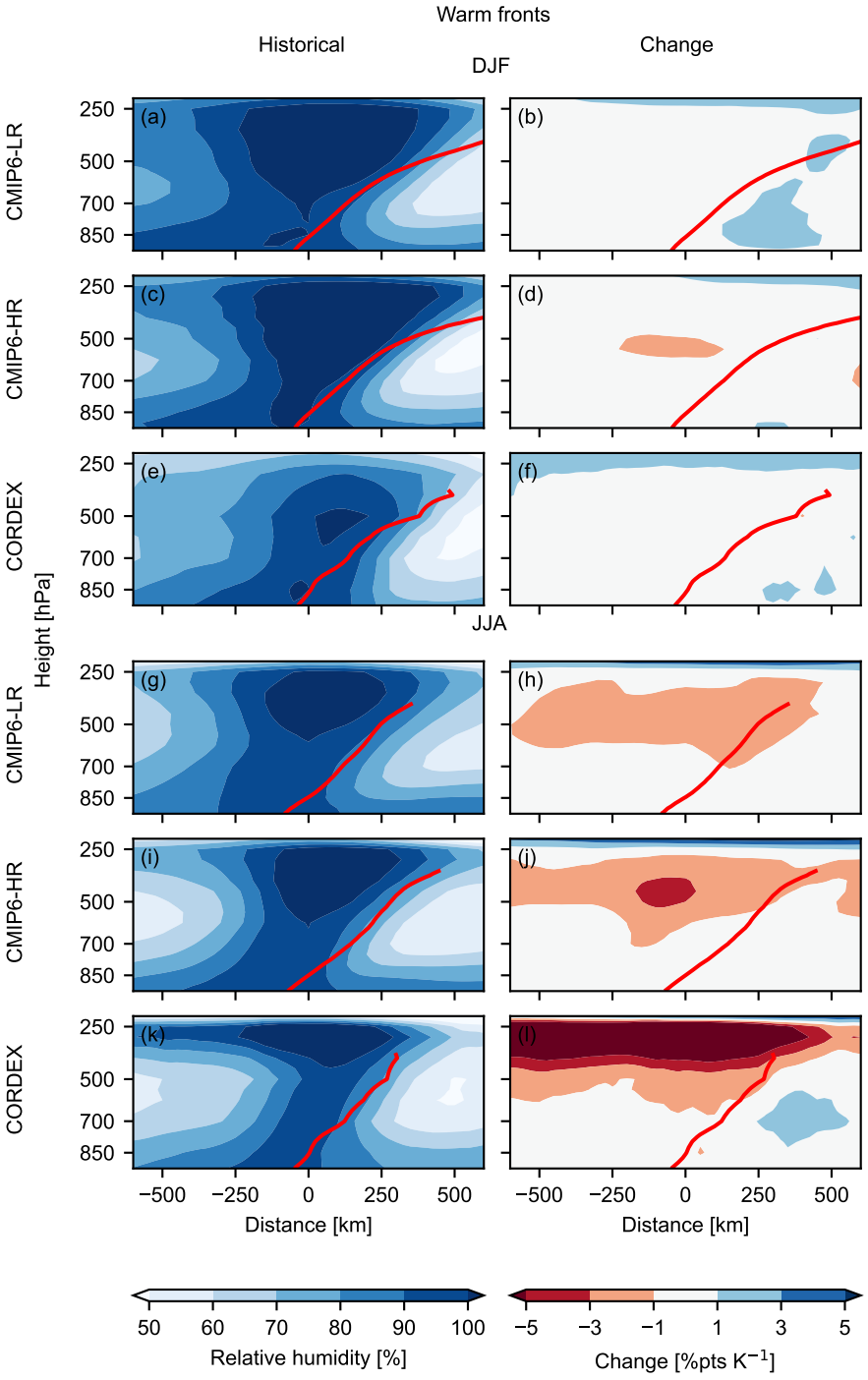

Figure S10. Same as Fig. S5, but showing relative humidity cross-sections of warm fronts of the NWEUR region.

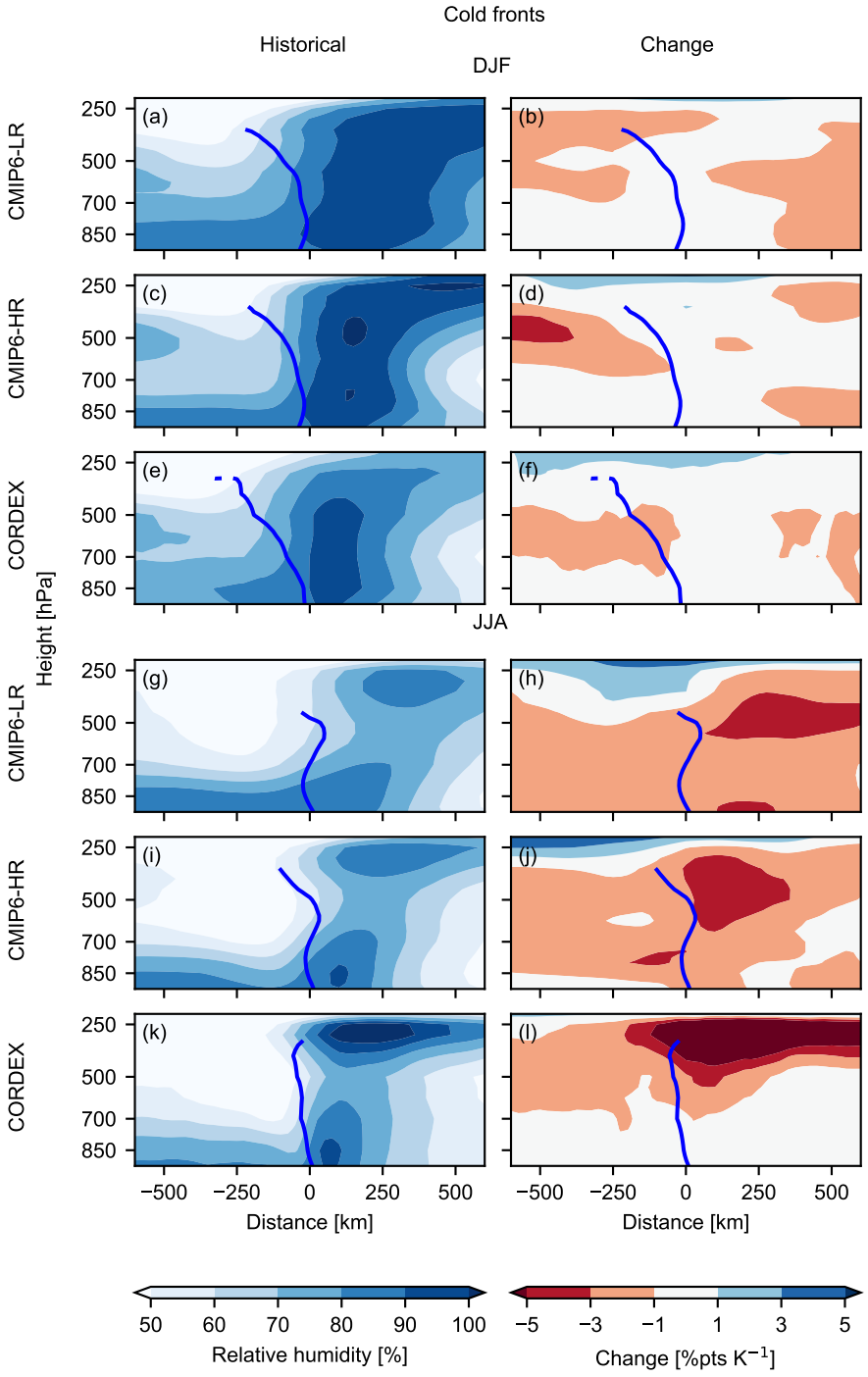

Figure S11. Same as Fig. S5, but showing relative humidity cross-sections of cold fronts of the SWEUR region.

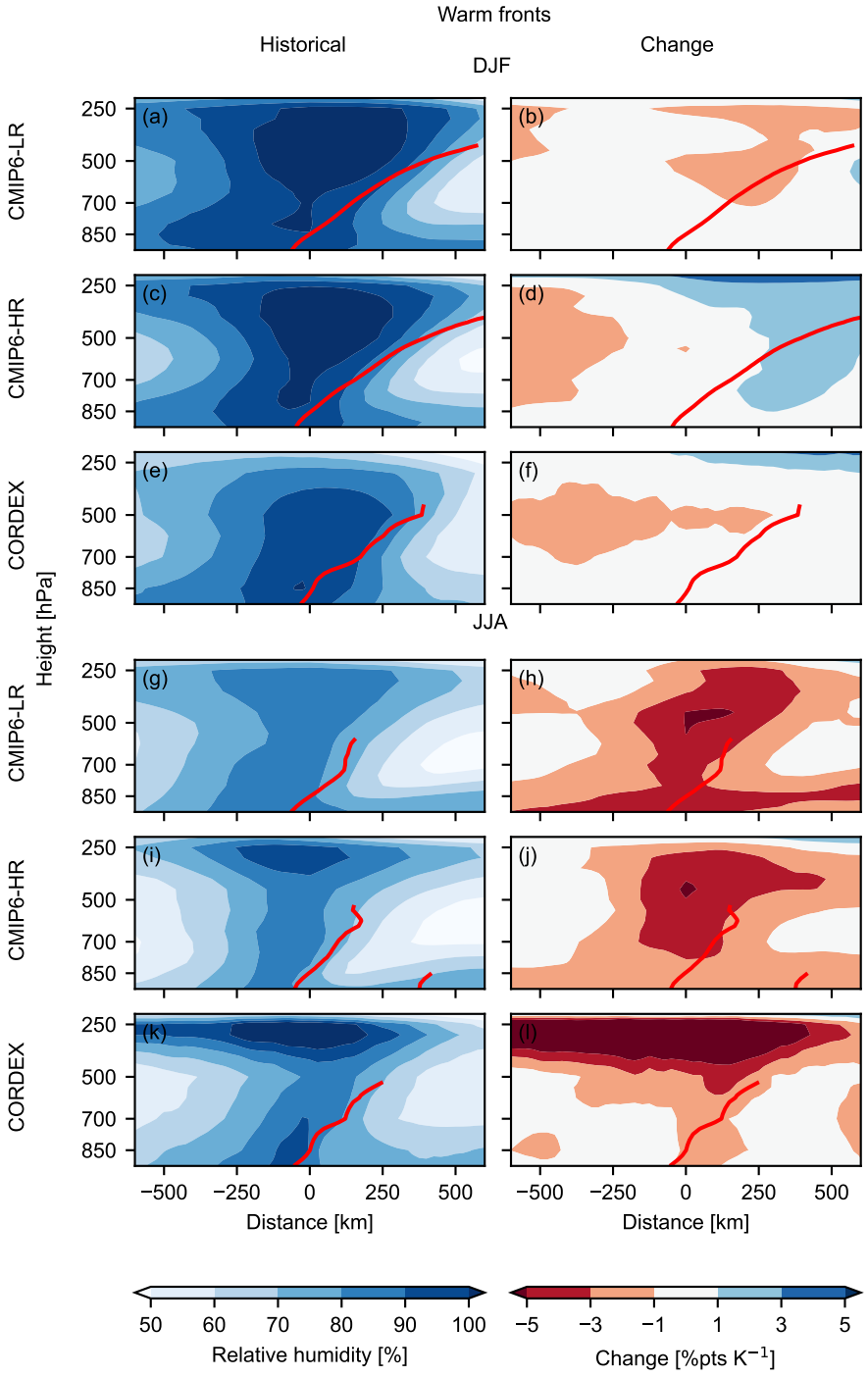

Figure S12. Same as Fig. S5, but showing relative humidity cross-sections of warm fronts of the SWEUR region.

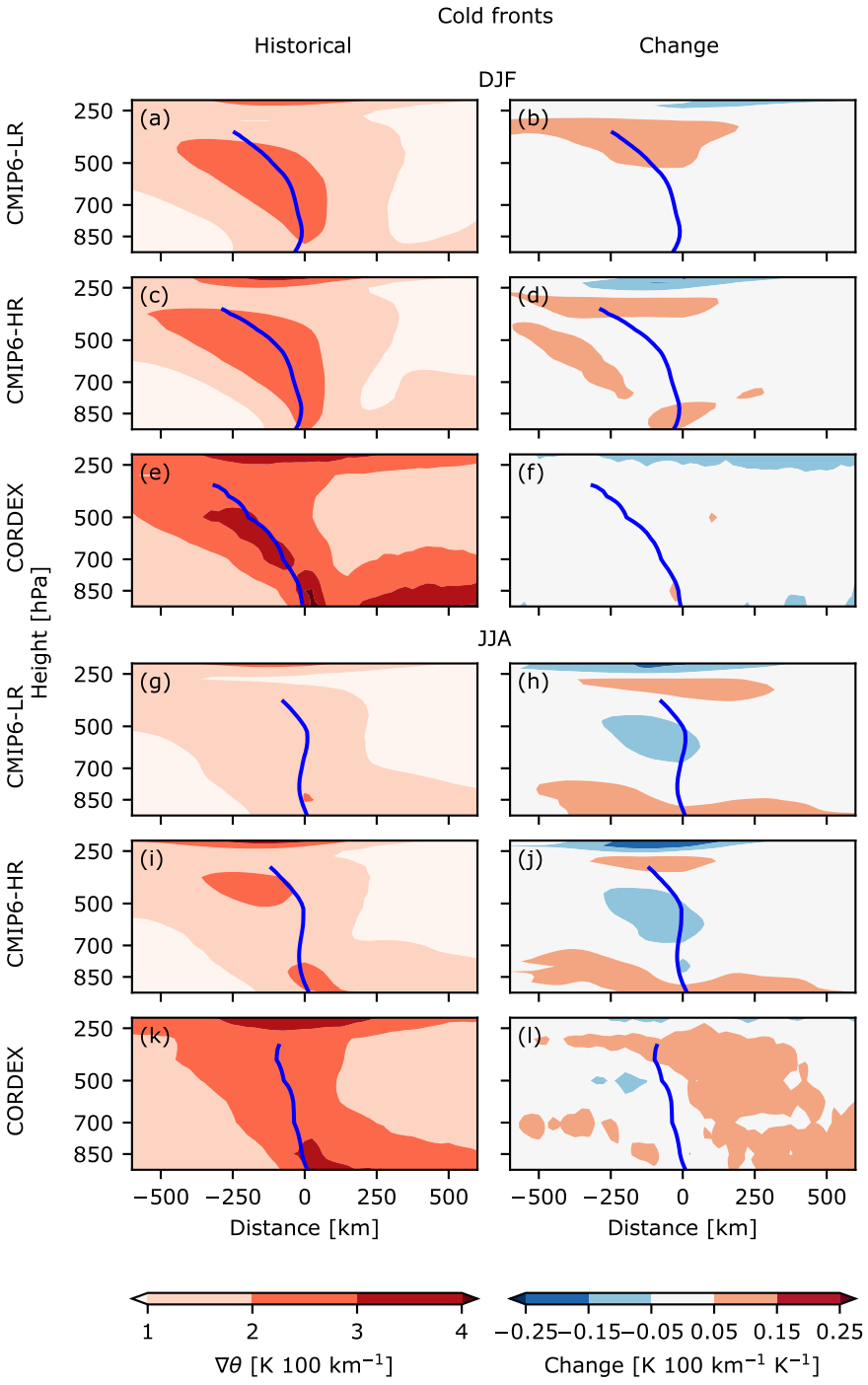

Figure S13. Same as Fig. S5, but showing $\nabla\theta$ of cold fronts.

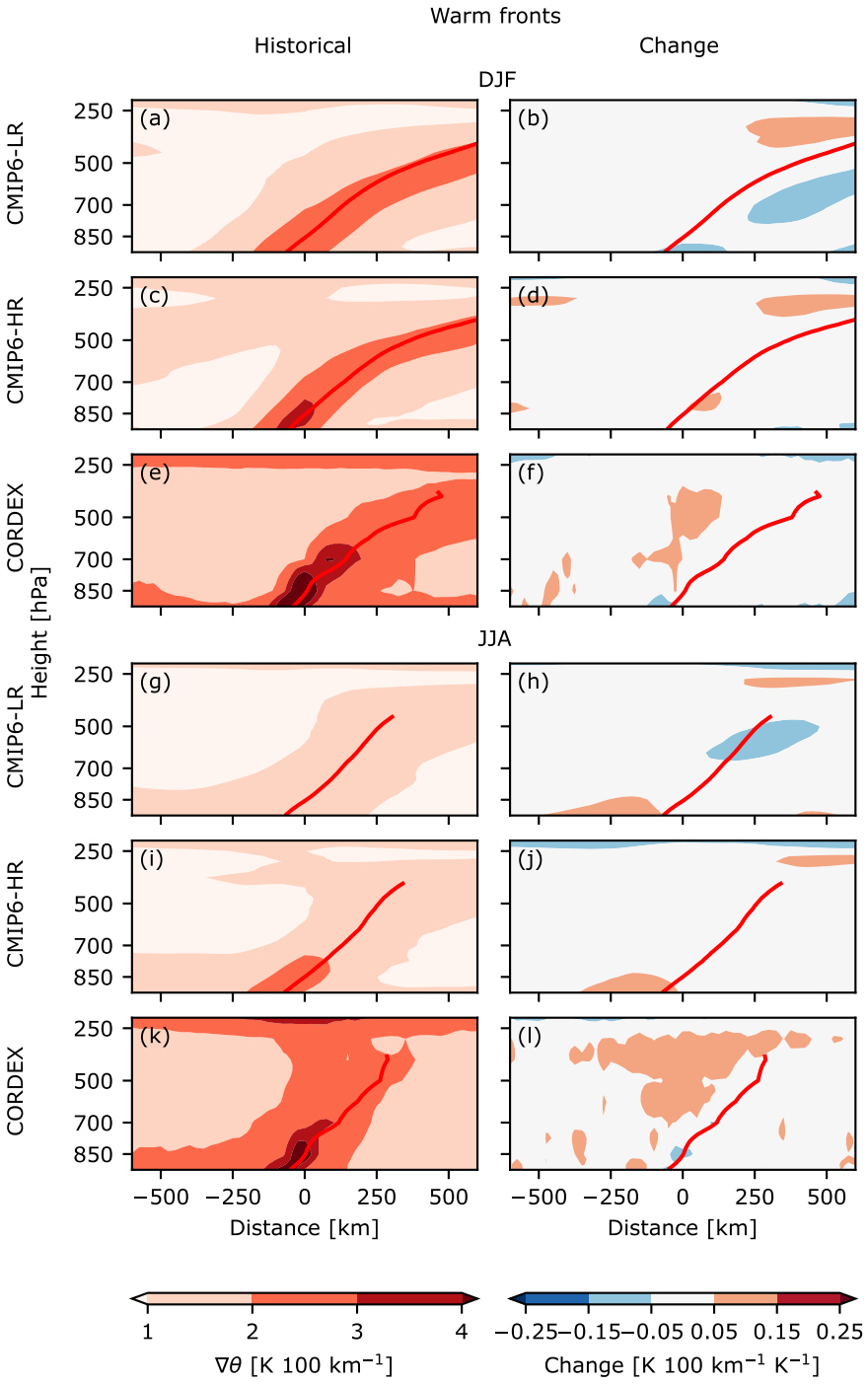

Figure S14. Same as Fig. S5, but showing $\nabla\theta$ of warm fronts.

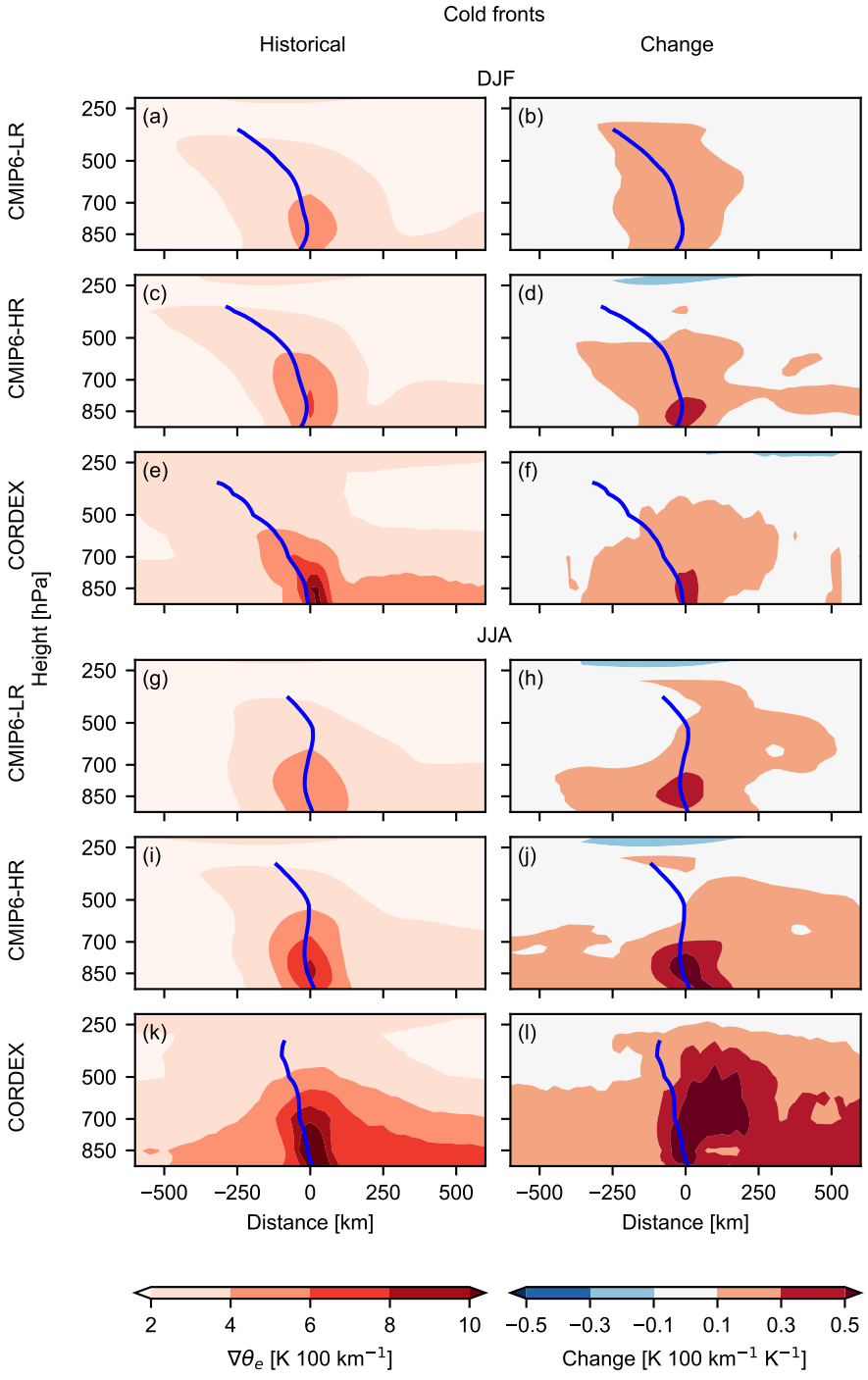

Figure S15. Same as Fig. S5, but showing $\nabla\theta_e$ of cold fronts.

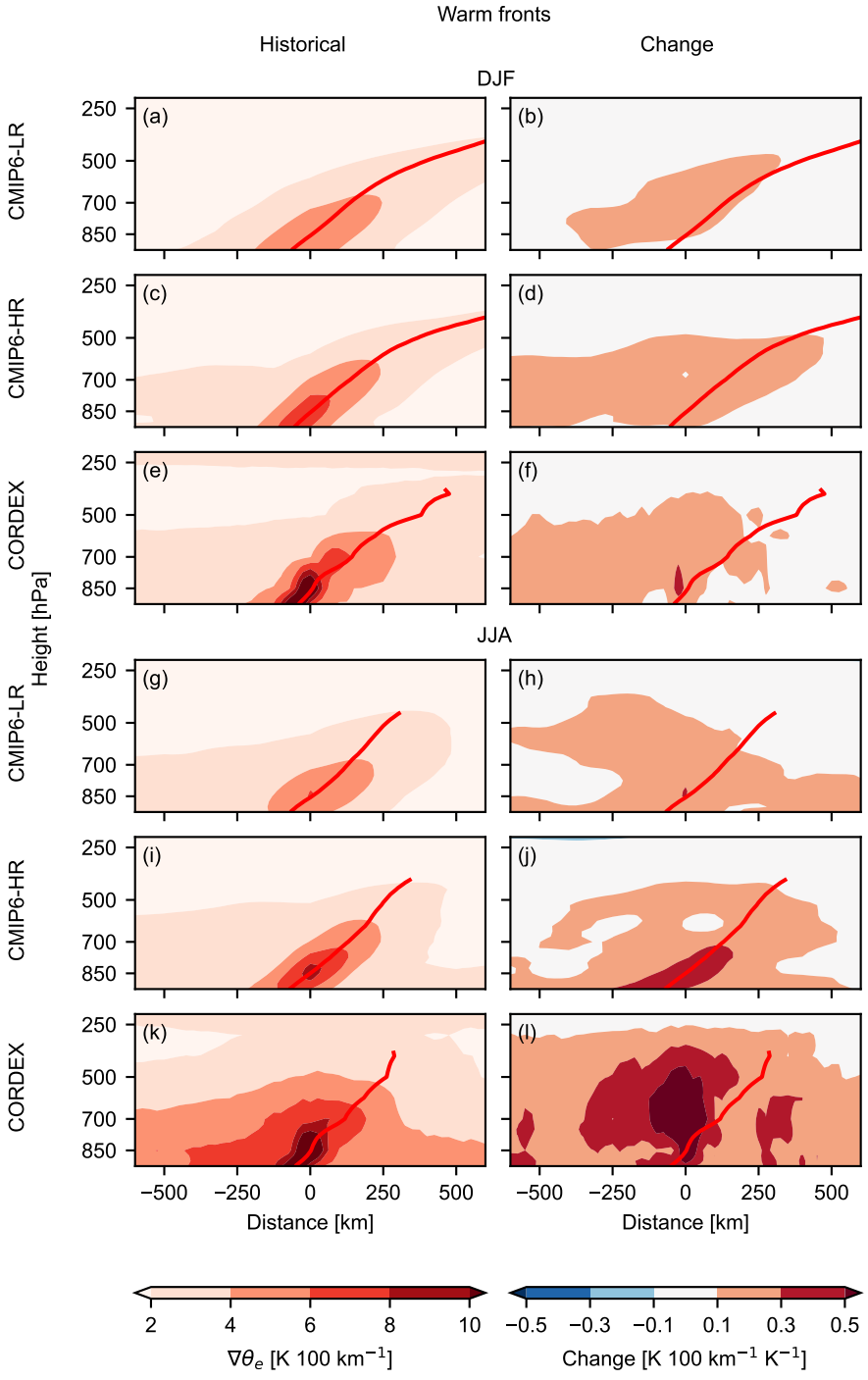

Figure S16. Same as Fig. S5, but showing $\nabla\theta_e$ of warm fronts.

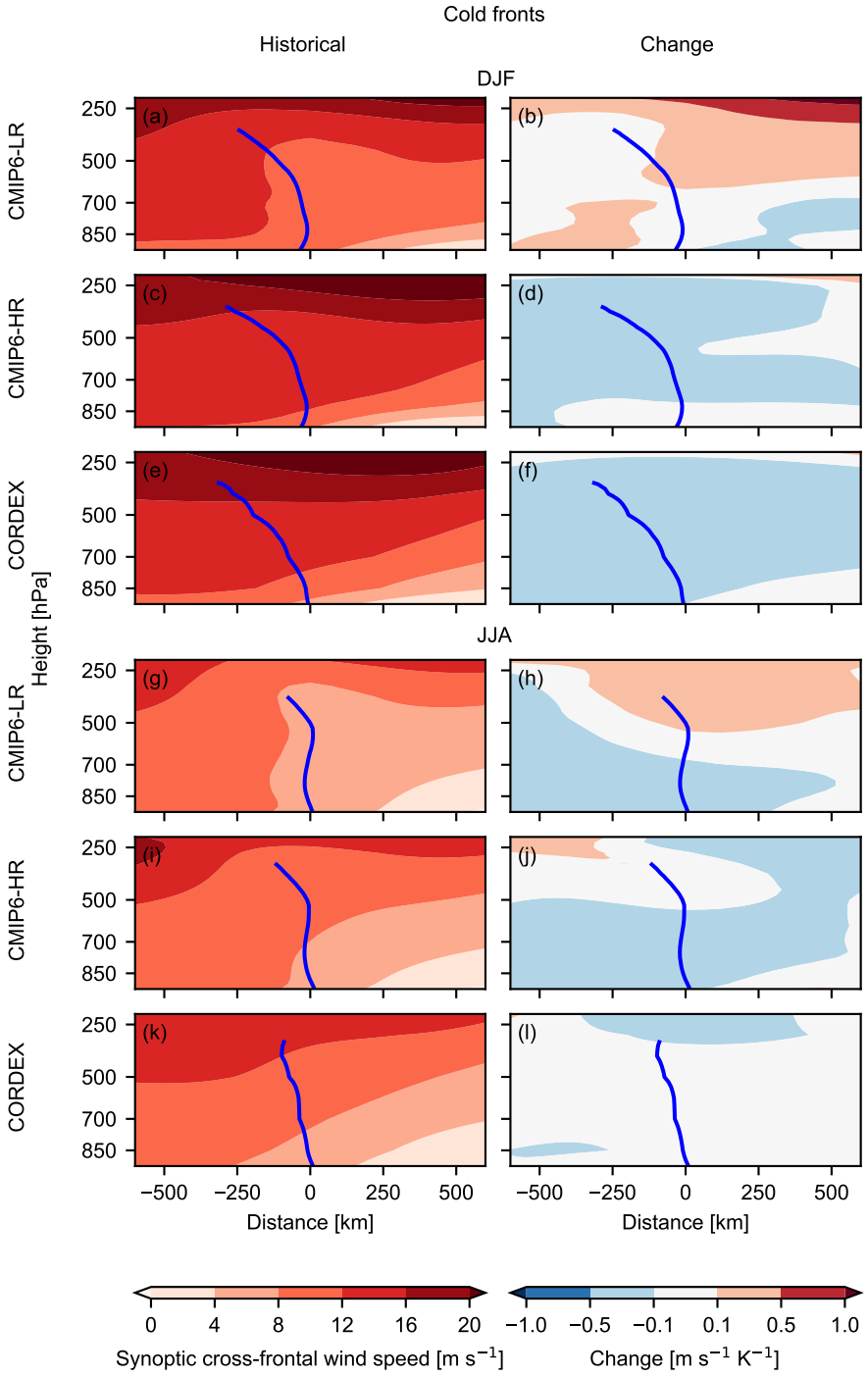

Figure S17. Same as Fig. S5, but showing synoptic cross-frontal wind speed of cold fronts.

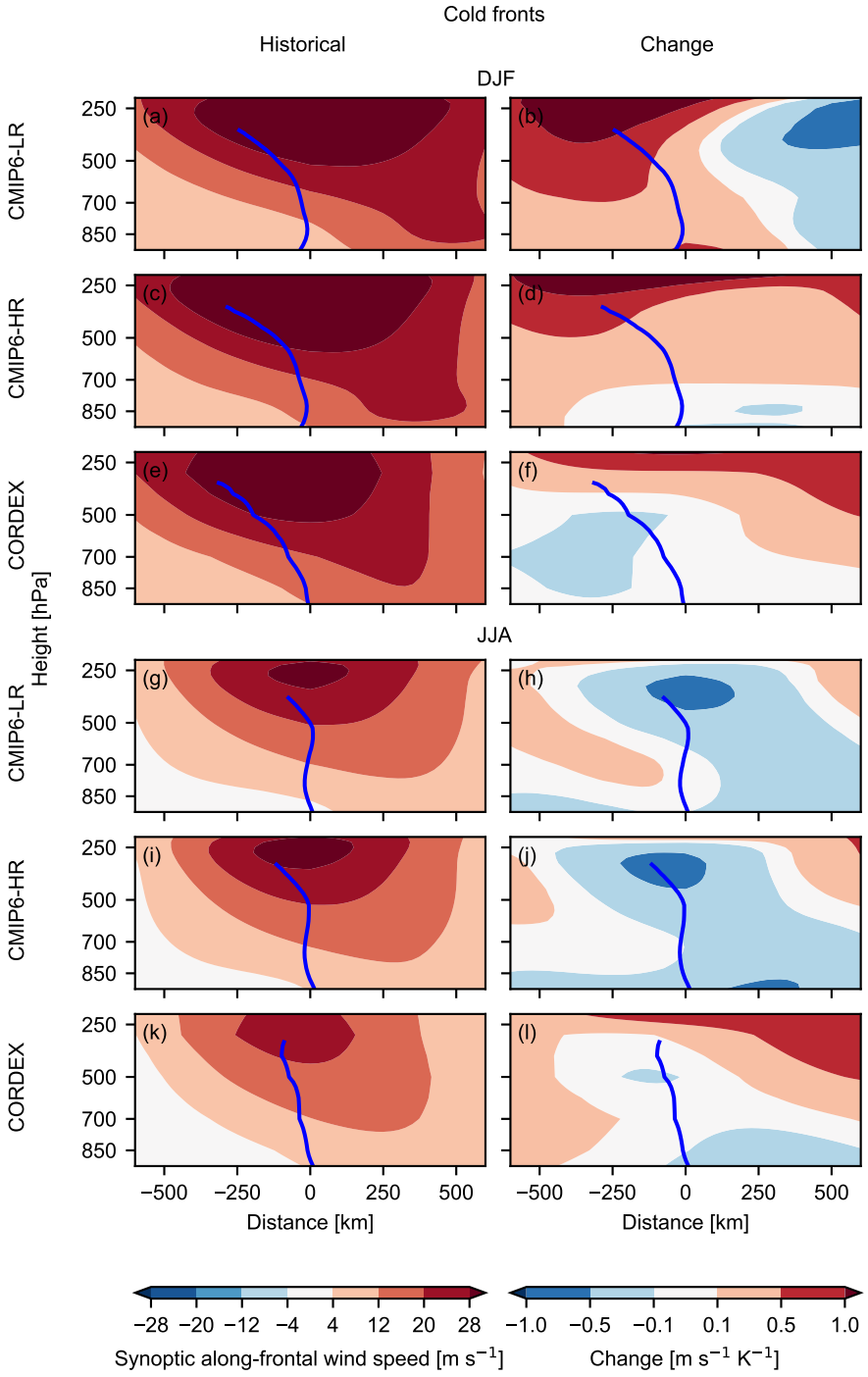

Figure S18. Same as Fig. S5, but showing synoptic cross-frontal wind speed of warm fronts.

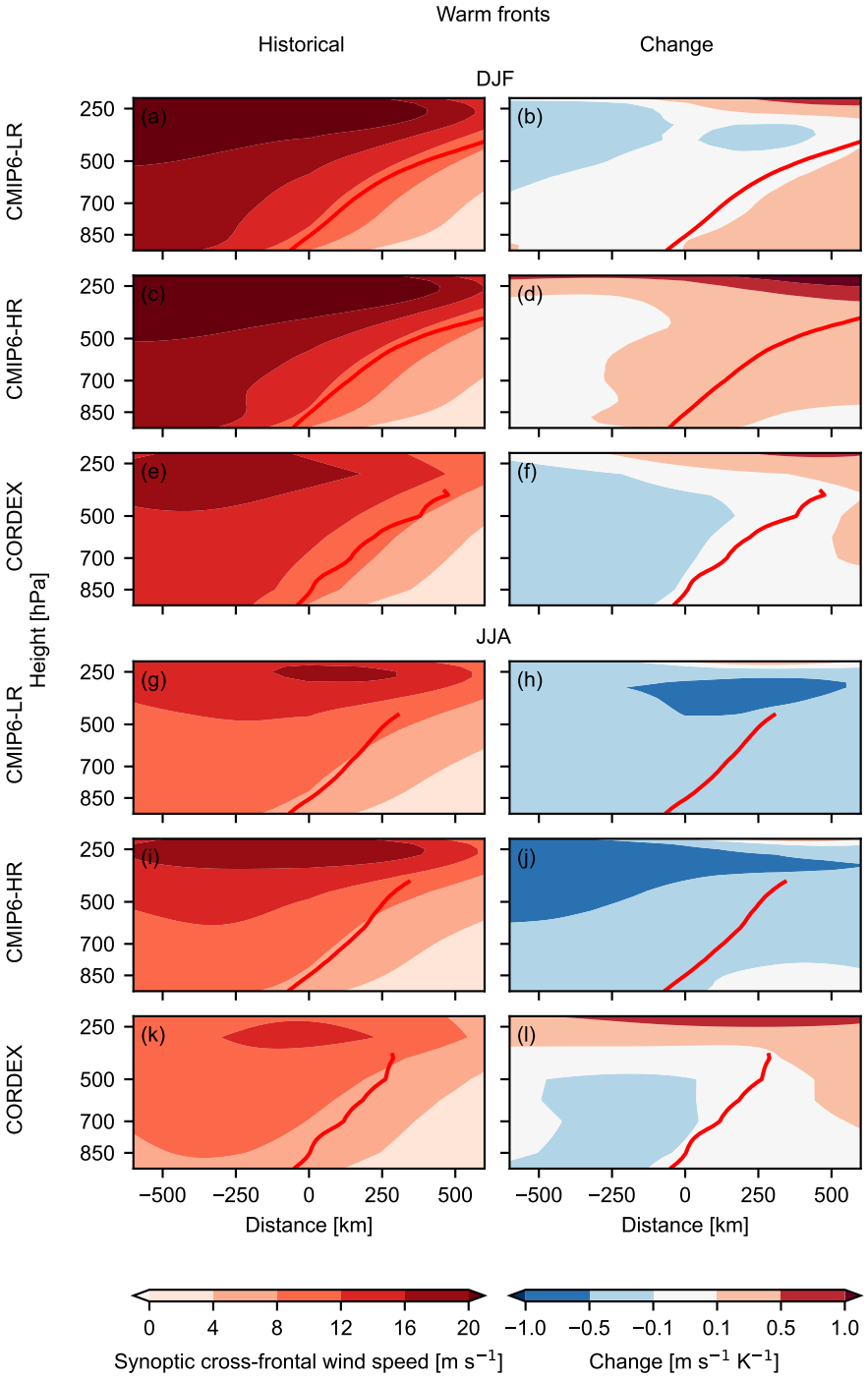

Figure S19. Same as Fig. S5, but showing synoptic along-frontal wind speed of cold fronts.

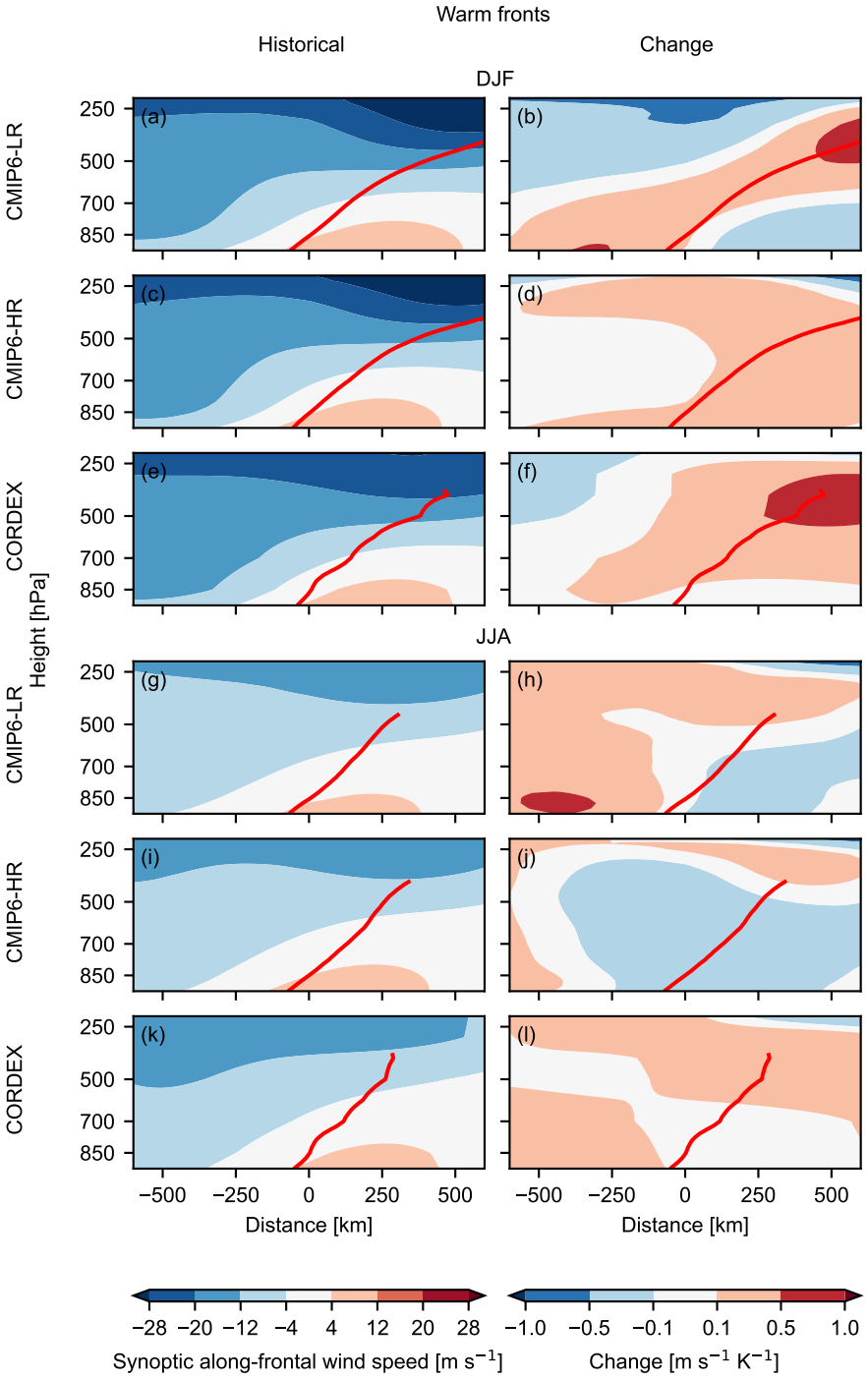

Figure S20. Same as Fig. S5, but showing synoptic along-frontal wind speed of warm fronts.